Probing the Interaction of T7 RNA Polymerase with Promoter†

Srin Sastry* and Barbara M. Ross

Laboratory of Molecular Genetics, Box 174, The Rockefeller University, 1230 York Avenue, New York, New York 10021

Received October 7, 1998; Revised Manuscript Received January 28, 1999

ABSTRACT: Transcription is the fundamental process by which RNA is synthesized by RNA polymerases on double-stranded DNA templates. One structurally simple RNA polymerase is encoded by bacteriophage T7. T7 RNA polymerase is an excellent candidate for studying structural aspects of transcription, because unlike the eucaryotic and bacterial RNA polymerases, it is a single subunit enzyme and does not require additional factors to carry out the entire process of transcription from start to finish. An important advantage of studying transcription using this enzyme is that the high-resolution crystal structure of T7 RNA polymerase has been solved. However, a cocrystal structure of the polymerase complexed with promoter has not yet been published. Here, we have used cross-linking techniques to understand the interaction of promoter with T7 RNA polymerase. We constructed promoters that were substituted with the photo-cross-linkable nucleotide 5-iodo uracil at every dT in the promoter from −17 to −1. This substitution replaces the 5-methyl in dT with an iodine atom. The substituted promoters were photo-cross-linked to T7 RNAP, and the efficiency of cross-linking was quantitated at every position. In the melting domain, the strongest contacts occurred at −3 and at −1 on the template strand while very weak cross-linking was seen at −2 and at −4 on the nontemplate strand. In the binding domain, the strongest contacts were seen at −16, −15, and −13 and at −10 on the template strand while at −17 and −14 on the nontemplate strand very weak cross-linking was observed. Cross-linking was poor in the intervening region between the binding and the melting domains. These results suggested that, in the T7 RNA polymerase−promoter complex, the polymerase molecule mainly contacts the template bases in the TATA box while the upstream contacts are used as an anchor for DNA binding. For a systematic study designed to probe the nature of base-specific interactions in the polymerase−promoter complex, we used neutral salts from the Hofmeister series. In general, the order of perturbation was sulfate > citrate > acetate for anions and ammonium > magnesium > potassium for cations. Using acrylamide, a neutral hydrophobic agent to probe for nonionic contacts, we observed that at −2, −4, and −17 the contacts had a hydrophobic component, while at many other positions there was no significant effect, suggesting that the contacts in the promoter−polymerase complexes were predominantly ionic but at certain positions nonionic interactions also existed. To localize a specific interaction in the melting domain, we proteolyzed the cross-linked T7 RNAP and analyzed the fragments using gel electrophoresis, mass spectrometry, and amino acid composition. High-resolution mapping indicated that amino acid residues 614−627 may be in the vicinity of the melting domain. Specifically, Y623 may contact −3 on the template strand.

T7 RNA polymerase (98.8 kDa) is a single-subunit protein that has been one of the most intensively studied RNAPs (*1*, *2*). T7 RNAP[1] initiates transcription on two main classes of promoters in the T7 phage genome, viz., class II and class III (*2*). In vitro, class III promoters are stronger than class II promoters. The class III promoter is a 23 bp highly conserved region (−17 to +6) that includes the +1 start site (*3*). The most striking feature of the promoters is the absolute requirement for guanine at +1 position (*2*). T7 RNAP binds specifically to the class III promoters with a relatively weak macroscopic affinity constant (K_{eq}) equal to ∼(2−5) × 10^7 M^{-1} (*4*−*6*). The polymerase−promoter complex stability depends on template conformation (*7*). Promoter binding apparently occurs at an extremely rapid rate approaching the diffusion limit (*8*, *9*). Promoter-T7 RNAP complexes have been characterized using footprinting, enzyme assays, mutagenesis, and gel shifts (e.g., see refs *4*, *7*, and *10*−*13*). Hydroxyl radical footprinting has revealed that the polymerase contacts predominantly one face of the promoter (*13*) while low-resolution NMR studies indicated that both faces of the DNA helix are contacted by the enzyme in the binding region (*14*). The T7 RNAP promoter has been functionally analyzed using site-specific mutagenesis and chemical modification (*5*, *12*, *15*−*17*). Site-directed mutagenesis has revealed that base changes in the binding domain (−17 to −5) minimally affected the rate of transcription initiation, while base changes in the initiation domain (−4 to +6) appear not to affect enzyme binding to promoter. These

† This work was supported in part by a Hewlett-Packard Company instrumentation grant.

* To whom correspondence should be addressed. Phone: 212-327-8987. Fax: 212-327-8651. E-mail: sastrys@rockvax.rockefeller.edu.

[1] Abbreviations: aa, amino acid(s); amu, atomic mass unit(s); ds, double stranded; 5-IU, 5-iodouracil; 4-HCCA, 4-hydroxy-α-cyanocinnamic acid; MALDI-TOF, matrix-assisted laser desorption ionization−time-of-flight; nt, nucleotide(s); ss, single stranded; T7 RNAP, bacteriophage T7 RNA polymerase; TEAA, triethylammonium acetate; XL, cross-links.

10.1021/bi9823941 CCC: $18.00
Published on Web 03/30/1999

findings have led to the functional partitioning of the promoter into a binding domain (−16 to −5) and a melting-initiation domain (−3 to +6) (*5*, *16*, *18*−*20*). T7 RNAP was proposed to "read out" functional groups in the promoter major and minor grooves (*21*). Insertion of large artificial nonDNA linkers 3 or 4 bp upstream of the start site appear to have little effect on start site selection by the enzyme, whereas these artificial insertions immediately adjacent to the start site seem to affect the fidelity of start site selection (*22*).

During open complex formation, about 6 or 7 bp in the promoter are melted (*5*, *13*, *23*) with a second-order rate of $\sim 2 \times 10^7$ M^{-1} s^{-1} (*6*). There are at least three different models regarding the mechanism of T7 RNAP open complex formation. In our model, base pair opening near the initiation site (at −1) is favored and is faster compared to the upstream base pairs (−4) (perhaps accounting for the rapid initiation without a lag phase) and the initiating GTP alters the rate of base pair disruption (*5*, *6*). A second model suggested that open complex formation was thermodynamically disfavored and that the rate of collapse of the open complex is competitive with transcription initiation and that the rate of opening was influenced by the initiating GTP (*24*). The second model directly contradicts a third model, which stated that promoter binding and DNA strand opening occurred almost simultaneously and quantitatively in a facile manner at extremely rapid rates, approaching the diffusion limit (*8*). The second proposal is more in consonance with our model (*5*, *6*) in which binding is followed by DNA strand opening, and base pair disruption may be somewhat slower in the presence of GTP—perhaps reflecting the competition between collapse of the open complex and transcription initiation. At any rate, the mechanism of open complex formation is still not clearly understood and a physical basis for it is lacking.

The crystal structure of T7 RNAP showed a protein of high α-helicity with a deep cleft (*25*). This original crystal structure contained many errors and a new crystal structure (complexed with T7 lysozyme) has now been published (*26*). However, the overall shape of the T7 RNAP molecule is the same in both models. The T7 RNAP structure bears a striking similarity to *Escherichia coli* DNA polymerase Klenow fragment and HIV-1 reverse transcriptase (*27*, *28*). The T7 RNAP crystallographic model, like the other polymerases, is shaped in the form of a cupped right-hand consisting of fingers, palm, and thumb. A "specificity loop" region (amino acids 742−773) may participate in stabilization of the promoter−polymerase complex and/or in promoter recognition (*20*). The thumb subdomian may contact the DNA to stabilize the ternary complex during processive elongation (*29*, *30*).

Earlier, we demonstrated by photochemical cross-linking that the promoter indeed binds in the cleft (*31*) and that the fingers subdomain recognized ss DNA (*31*, *32*). We speculate that a portion of the fingers subdomain may participate in establishing or maintaining an open DNA for transcription. A portion of the N-terminal domain makes contacts with nascent RNA (*33*). Here, we asked the following question: how does the polymerase contact the different base positions in the binding and melting regions of the promoter? To address this question, we pursued a cross-linking approach. We substituted dT with 5-IU at all permissible positions in the binding and the melting domains of a T7 promoter and cross-linked the polymerase to the IU positions. Using high-resolution methods, we mapped the amino acid residues in the polymerase that contacted the −3 position in the promoter's melting domain. On the basis of this and other work, we present a view of the promoter−polymerase complex.

MATERIALS AND METHODS

DNAs and Proteins. DNA oligonucleotides were purchased from Operon Technologies (Alameda, CA) and were further purified by anion-exchange HPLC (*34*). The concentrations of the DNAs were measured by UV absorbance ($\epsilon_{260} = \sim 10^4$ M^{-1} cm^{-1} per nt). We purchased the promoter sequence 5′-TAATACGACTCACTATAGGGAGA-3′, which contained either dT (wild-type) or 5-IU in place of dT at various positions (see Figure 2). Oligonucleotides were 5′-end labeled using [γ-^{32}P]ATP (Sp. radioactivity, 6000 Ci/mMol) and T4 polynucleotide kinase (*35*). T7 RNAP was prepared locally according to published procedures (*36*, *37*). The concentration of the purified T7 RNAP was determined using $\epsilon_{280} = (1.4 \pm 0.1) \times 10^5$ (*36*).

Small-Scale Cross-Linking Reactions. Equimolar concentrations (1−10 μM) of two complementary DNA promoter strands (only one of which had an IU at a specific base in place of dT) were mixed in buffer containing 10 mM Tris-HCl (pH 7.5) + 1 mM EDTA + 1 mM $MgCl_2$ and heated at 70 °C for 5 min and then slowly cooled to room temperature over a period of 2−3 h. The ^{32}P label was always present in the strand containing the IU in the ds promoter. Typically 1−10 pmol of ds IU-promoters were mixed with 3−30 pmol of T7 RNAP in binding buffer (50−300 μL), which consisted of 30 mM Hepes, pH 7.8, 100 mM K glutamate, 15 mM Mg $(OAc)_2$, 1 mM DTT, and 0.05% Tween-20 (*38*), and incubated at 37 °C for 10 min for polymerase binding to occur. The reactions were then irradiated with 300−308 nm UV ($\sim 4 \times 10^{17}$ quanta/mL/min) in a Rayonet photochemical reactor (Southern New England Ultraviolet Co., Bradford, CT) for 15 min. Gel-loading sample buffer was added, and the samples (containing SDS at 1%) were heated in boiling water bath for 5 min and run on 10% acrylamide−SDS Bio-Rad mini-gels or on larger gels (12 cm L x 16 cm W). The gels were dried and autoradiographed. In X-ray film or phosphor images of the dried gels, the DNA-protein cross-links were represented by radioactive bands that migrated less rapidly compared to non-cross-linked [^{32}P]DNA, which was usually found at the bottom the gels. For digestion of the cross-links with proteases, the irradiated reactions were first precipitated with saturated $(NH_4)_2$ SO_4 and then redissolved in water. Proteolysis was carried out as recommended by the manufacturer of the proteases (Promega, Madison, WI). Proteolyzed fragments were run on Tris-glycine gels (see Figure 3 legend) and the fragments were sized using Bio-Rad protein standards (catalog no. 161-0305/0309) and the proteolytic fragments from non-cross-linked T7 RNAP (size determinations were within ± 200−500 Da).

Large-Scale Cross-Link Purification and Microchemical Analyses. The cross-linking reactions were scaled up for two batches, each containing 10 mg of T7 RNAP and run on 10% acrylamide−SDS preparative gels. The cross-links were identified by autoradiography using X-ray films that were

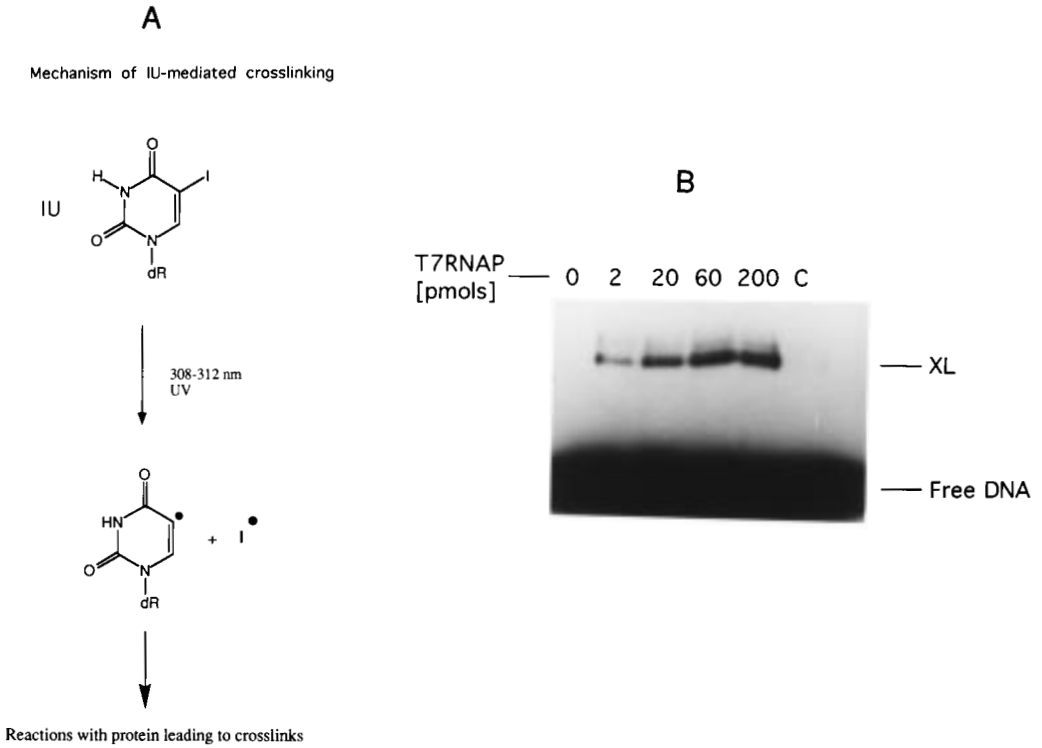

FIGURE 1: (A) The structure of 5-iodo uracil and the important points regarding the mechanism of cross-linking. (B) 6% acrylamide−SDS gel showing cross-linking of a promoter to various amounts of T7 RNAP. The promoter contained a single 5-IU at −1 position. C = control, i.e., sample without UV. XL indicates cross-links.

exposed to the wet gels. The bands containing the cross-links were excised as very small gel pieces and were then digested in situ with trypsin for 24 h. The proteolyzed fragments were eluted passively and/or by electro elution. The eluted DNA-*cross*-linked peptides were first adsorbed on to strong quaternary amine anion-exchange filters (as recommended by the manufacturer, Sartorius, New York), which strongly bind the DNA. The filters were then thoroughly washed with 10 mM KCl/water to remove loosely bound peptides, and the cross-linked fragments were eluted with 1 M KCl, dialyzed extensively against water, and lyophilized to semidryness. Additional purification was carried out by HPLC procedures similar to those described in our previous work (*31*, *32*). The peaks of interest were identified by their absorption spectra and by the presence of the ^{32}P label (*31*, *32*). MALDI-TOF mass spectrometry was done using 4-HCCA as the matrix (*39*, *40*) in a VOYAGER-RP (PerSeptive Biosystems, Farmingham, MA) workstation. The instrument was calibrated using external protein standards (from PerSeptive Biosystems) and an internal standard (lysozyme). Mass determinations were accurate to less than ±5 amu in the 2−15 kDa linear mass range.

RESULTS AND DISCUSSION

Cross-linking has traditionally offered a very powerful chemical approach to mapping protein−DNA interactions in solution. Cross-linking studies have either confirmed some structural details of NMR or crystallographic models or have mapped additional DNA-binding protein domains and motifs (e.g., refs *41*−*43*). The distinctive feature of photo-cross-linking reactions is that they occur most often when the interatomic/molecular distances are within the van der Waal's volume/radii of photo probes, implying that, under appropriate conditions, the positions of the cross-links can be interpreted as physical contact(s) between two entities. Here we used 5-IU as a cross-linking agent to study the contacts between T7 RNAP and a promoter.

Cross-Linking of T7 RNAP to IU Promoter. We substituted 5-IU at every permissible position (i.e., dT) in the binding and melting domains. To test the effect of 5-IU substitution on transcription, we compared G-ladder synthesis on an IU-containing promoter at −3 with that on a wild-type promoter. This assay did not reveal any significant differences between the two promoters either in terms of relative quantities or qualities of the patterns of poly rG ladders (not shown). A similar result was obtained with IU substitution at −1. Therefore, we concluded that IU had very little or no effect on transcription initiation. These results were not surprising because 5-IU does not distort DNA to a significant extent. The van der Waals radius of iodine (2.15 Å) is similar to that of the CH_3, which it replaces in dT (see Figure 1A). The C5 iodine atom in IU is in the major groove, as is the CH_3 of dT. An attractive feature of IU-mediated protein-DNA cross-linking is that cross-linking yields are quite reasonable (5−15%) and that cross-linking occurs by a fairly simple, efficient, and well-characterized photochemical mechanism (Figure 1A). Cross-linking may be mediated by a singlet π,π^* state (analogous to BrU), bond homolysis, and radical formation (Figure 1A). Through this mechanism, one IU residue cross-links to one amino acid side-chain atom. The details of the mechanisms have been very well worked-out (e.g., see refs *44*−*46*). Figure 1B is an example of an acrylamide−SDS gel showing that cross-link yield increased linearly with increasing amounts of T7 RNAP added to a fixed amount of IU promoter. The cross-link (XL) is indicated by the intense major band, which runs less rapidly

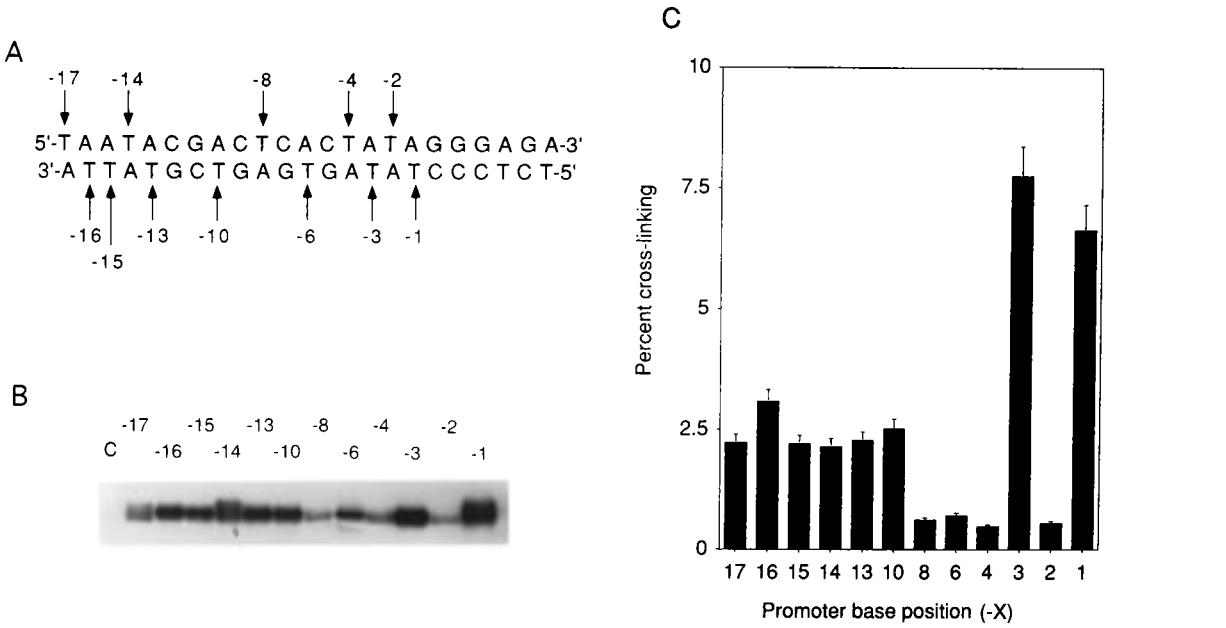

FIGURE 2: (A) Sequence of a promoter that was used in this work. The arrows indicate the positions of the 5-IU substitutions. (B) Bands from an SDS gel showing cross-links at each substituted promoter position. C = control, i.e., sample without UV. (C) Quantitation of cross-linking efficiency at each position. The data were computed from phosphor counts in gels such as that in panel B. Percent cross-link = {[phosphor counts in cross-links]/[phosphor counts in cross-links + phosphor counts in free DNA]} × 100. The phosphor counts were corrected for background counts.

compared to the free DNA band. The very faint band located just above the major band may represent either a very minor alternate state of the denatured protein−DNA cross-link during its migration in the SDS gel or a photoreaction at an alternate secondary site in the protein. Control cross-linking reactions were carried out using either nonpromoter ds DNA or ss DNA oligos (not shown). In both cases, either there was no cross-linking or there were very faint, multiple, diffused cross-link bands, which suggested nonspecific cross-linking. This result is probably due to the well-known nonspecific binding activity of T7 RNAP to nonpromoter DNA and to ss DNA (*32*, *47*). In competition experiments performed with a ^{32}P-labeled −3 IU substituted ds promoter DNA and with an excess of unlabeled nonspecific ds or ss DNA, we observed only strong, sharp, and specific cross-link bands (not shown). These results indicated that cross-linking was a due to the specific interaction of T7 RNAP with the ds promoter DNA.

Next, we constructed class III promoters with 5-IU in place of dT from −17 to −1 (Figure 2A). Each IU substitution was made in a separate template. In principle, IU-mediated cross-linking of singly substituted promoters could reveal the differences in strength/proximity of base by base contacts between promoter and T7 RNAP, assuming that the cross-linking mechanism is the same at every base substitution. The limitations of this approach are that information regarding contacts at unsubstituted positions of interest is excluded and that only the contacts in the major groove C5 position of dT are probably seen through cross-linking. A potential caveat is that since cross-linking cannot strictly be correlated to quantitative affinity (K_d), only qualitative conclusions can be made. Cross-linking was most efficient at −3 IU and at −1 IU on the template strand compared to the other sites in the promoter (Figure 2, panels B and C). There was a significant drop in cross-link yield at −2. The weakest contacts were at −8, −6, and −4. Between −17 and −10, total cross-linking yields were more or less uniform within experimental error, whether the substitutions were made on the template or nontemplate strand. In a previous study, where all the dTs were replaced with dUs (i.e., replacement of thymine CH_3 with an H), it was concluded that the thymine CH_3 groups were not a determinant in promoter-binding specificity between −17 to −13, (*48*). This conclusion was based on the measurement of the kinetic parameter K_m, which was assumed to approximate K_d. Footprinting on mutated promoters suggested that from −12 to −8 there was weak binding (*12*). Assuming that the greater the sharpness and intensity are of the cross-linked bands, the higher the strength and proximity of contacts; between −17 and −10, the template strand contacts appear to be more homogeneous than the nontemplate strand cross-links (Figure 2B). It has been shown that −10/−11 bp probably contact N748 (*49*). The kinetic parameter K_m suggested that position −10T on the template strand was not directly involved in contacts (*21*, *48*). The strong cross-link band due to the −10 IU on the template strand appears to indicate that there is indeed a contact (Figure 2, panels A and B). Using site-directed mutagenesis, it was shown that Q758, which is in the specificity loop (Figure 6), contacted −8 bp (*20*). We could not assay for cross-linking at −8 on the template strand because it is dA. The 6-amino of −8A on the template strand (Figure 2A) is an important contact (*19*). On the basis of in vitro enzyme kinetics, the −8 dT methyl on the nontemplate strand was previously shown not be involved in polymerase contacts (*48*). However, our result appears to indicate that there is a weak contact with nontemplate strand at this position (Figure 2). Our finding agrees with results from mutagenesis showing that a T to A substitution at −8 on the nontemplate strand reduced promoter activity in vivo (*50*), implying an interaction at this position. The 5-methyl group at −6T on the template strand was shown to be a major groove contact determinant (*19*). Cross-linking of −6 IU on the template strand indicates that there is indeed a contact (Figure 2ABC). In the "TATA" box (−4 to −1; Figure 2A)

Table 1: Summary of the Effects of Ionic and Nonionic Agents[a]

base position in promoter	anions[b]	cations[b]	acrylamide[c]
−1	sulfate ≥ citrate > acetate	$NH_4^+ > Mg^{2+} > K^+$	N
−2	sulfate ≥ citrate > acetate	$NH_4^+ \geq K^+ > Mg^{2+}$	++
−3	sulfate ≥ citrate > acetate	$K^+ > Mg^{2+} > NH_4^+$	N
−4	sulfate ≥ citrate > acetate	$NH_4^+ > Mg^{2+} > K^+$	++
−6	sulfate ≫ citrate > acetate	$NH_4^+ > Mg^{2+} > K^+$	−
−8	sulfate ≫ citrate > acetate	$NH_4^+ \cong Mg^{2+} \cong K^+$	+
−10	sulfate ≫ citrate > acetate	$NH_4^+ > Mg^{2+} > K^+$	N
−13	sulfate > citrate > acetate	$NH_4^+ \cong Mg^{2+} \cong K^+$	−
−14	sulfate > citrate > acetate	$NH_4^+ > K^+ > Mg^{2+}$	+
−15	sulfate > citrate > acetate	$NH_4^+ \cong K^+ \cong Mg^{2+}$	N
−16	sulfate ≫ citrate > acetate	$NH_4^+ \cong Mg^{2+} \geq K^+$	+
−17	sulfate > citrate > acetate	$NH_4^+ > K^+ > Mg^{2+}$	++

[a] The results are summarized using the data acquired from phosphorimages of gels. [b] The average change in cross-linking value relative to the average value obtained without the agent, which was taken to be 100%. The agents are rated in decreasing order of their effectiveness in decreasing cross-linking. [c] N indicates no significant effect. Plus (+) or minus (−) indicates either an increase or a decrease in cross-linking relative to that in the absence of acrylamide.

near the start site of transcription, major contacts are at −3 and at −1 on the template strand (Figure 2, panels B and C). A previous model predicted that the methyl groups (here the I) of −4 T to −1 T were probably in the back face of the helix relative to the binding face in a standard B-DNA configuration (*13*). However, if the TATA region is melted in the open complex, the orientation of methyl groups in the DNA may be different compared to those in standard ds B-DNA. Here, cross-linking clearly shows that −1 and −3 are strongly contacted by the polymerase in the template strand (Figure 2, panels B and C). These results agree with the conclusions from a previous study, which showed that removal of the thymine methyl groups at −1 and at −3 altered the enzyme kinetic parameters relative to the wild-type promoter (*48*). However, removal of methyls at −2 and at −4 did not change the kinetic parameters (*48*). The binding constant was also not affected by a mutation at −4 (*12*). Both of these observations are in agreement with our result showing very weak contact, if any, with −2 and −4 bases (Figure 2, panels B and C).

Here, we have assumed that sharp, intense cross-link bands in the gel (Figure 2, panels B and C) reflect proximity of polymerase-base contacts while the diffused, less intense, multiple and clustered bands indicate weak or flexible contacts. Our results suggest that T7 RNAP may be positioned asymmetrically on the promoter with the rear end of the polymerase making anchored contacts at −16 and −15, and at −13 and −10 in the upstream binding domain. Segments of the polymerase front end strongly contact the −1 and −3 bases while the middle portion of the promoter from −8 to −4 on the nontemplate strand are weakly contacted or not interacted with at all (Figure 2C). Our results are consistent with hydroxyl radical footprinting data where protection was seen from −16 to −13 and between −3 and −1 on the template strand (*13*). The weak cross-linking at −8 and at −4 on the nontemplate strand, and the weak contact at position −6 on the template strand are also in agreement with the footprinting data. Our results are different from the OH radical footprinting results at position −10 IU on the template strand (Figure 2, panels B and C), where we see cross-linking but OH radical footprinting indicated no protection by the polymerase. On the other hand, at −10, OH radical footprinting data showed contact with the nontemplate strand. Here, it must be noted that we are concerned with cross-linking via the C5 atom facing the major groove while the OH radical attacks the sugars. The different results may be due to these different chemistries. Our results suggest a polymerase poised to initiate transcription with the strongest contacts at −3 and at −1 in the melting domain. Earlier, using fluorescence and psoralen-mediated promoter cross-linking, we suggested that bp −1 may open rapidly followed by −6 and −4 (*5*, *6*). In the present work, cross-linking efficiencies were in the order −1 ≈ −3 ≫ −6 > −4 (Figure 2, panels B and C). Assuming that the higher cross-linking efficiencies indicate a higher strength of contact, this result fundamentally agrees with our previous prediction based on fluorescence.

An alternative interpretation of the data in Figure 2, panels B and C, is that the differences in cross-linking yields may not actually reflect proximity and strength of binding but may be due to the differences in IU-photoreactivity. For example, IU-*cross*-links preferentially to Tyr, although Phe, Met, and His can also cross-link at much lower efficiencies (*46*, *51*, *52*). It is possible that between −17 and −10, where the cross-linking yields are fairly uniform (Figure 2C), IUs were cross-linked either to Tyr residues and/or to one of the other specific amino acids mentioned above. However, it is possible that at −3 and −1 IU, where cross-link yields are much higher than at other positions (Figure 2C), Tyr is involved in cross-linking. Conversely, poor cross-linking yields may simply suggest that one or the other amino acids that can preferentially cross-link may not be within the vicinity of IU. For these reasons, it is possible that, in our experiments, preferential photochemistry of the cross-linking agent may have affected the cross-link yields. Nevertheless, we believe that amino acid−base proximities, the strength of the contacts, *and*, to a certain extent, differences in photoreactivity may have contributed to the overall results. Therefore, we favor the idea that photo-cross-linking yields at different base positions in the promoter to some extent reflect the proximity and strength of individual base−amino acid residue contacts.

The Hofmeister Effect; Ionic and Nonionic Interactions. Protein−DNA interactions are strongly susceptible to neutral salts in moderate concentrations (0.1−1 M) because of their electrostatic and lyotropic effects. Electrostatic effects may depend on the ionic strength and sign of the charge. Lyotropic effects are mostly independent of the charge. These effects may stabilize or destabilize the native structure of macromolecules. Salts may alter the structure of water at protein−

DNA interfaces and/or influence the interactions between the negatively charged phosphate oxygens in DNA and the positively charged amino acid side chains (see refs *53*−*56* for reviews). The salts in the Hofmeister series are good candidates for a systematic approach to understand these effects. We tested some cations and anions in the Hofmeister series to ask whether a particular contact is ionic or not. To test for nonionic interactions, we used acrylamide as a probe. The decrease in cross-link yield was quantitated for each IU substitution using phosphor images of cross-linked bands in SDS−polyacrylamide gels (data not shown). The results from these data are summarized in Table 1. As discussed above, the salt effects are probably quite complex. But some general conclusions can be drawn from Table 1. The magnitude of the effect is more predominant with anionic competitors than with the cationic competitors. In general, the Hofmeister effect holds for the anions, i.e., SO_4^{2-} > citrate > OAc in reducing cross-linking at each promoter base position (Table 1). With respect to the cations, it appears that NH_4^+ competes more effectively than Mg^{2+} or K^+ at many positions except at −3, where K^+ and Mg^{2+} are the more effective competitors. These results may suggest that ionic interactions strongly influence either by directly affecting cross-linking and/or indirectly by modifying the microenvironment of the interactions at the polymerase−promoter binding interfaces. Some interactions may involve salt bridges between DNA backbone phosphate oxygens and basic side chains, which may be competed out by the probing agent. Surprisingly, acrylamide, a neutral hydrophobic molecule, increases cross-link yield up to 2-fold at certain positions (Table 1). This may indicate a hydrophobic (nonionic) effect that is involved in some contacts. At other positions, either there was no effect (N in Table 1) or there was a slight decrease (minus sign in Table 1). In summary, while anionic and cationic interactions are involved in promoter binding, hydrophobic effects do influence the contacts at certain positions, specifically at −2, −4, and −17.

Mapping Polymerase Regions Interacting with the Melting Domain of Promoter. To map a contact in the melting domain of promoter, we specifically placed IU at −3 in the template strand. Cross-linking was carried out first on a preparative scale, and then the cross-linked T7 RNAP was digested with several types of proteases to assess the stability and the complexity of the cross-link digestion pattern. A large number of discrete and stable radiolabeled fragments were seen with a number of proteases. Figure 3 is an example of an autoradiogram of a polyacrylamide−SDS gel showing the partial proteolytic digestion pattern obtained with −3 IU promoter cross-linked to T7 RNAP. Both clostripain (endoproteinase Arg-C, which cuts on the carboxyl side of arg) and endoproteinase lys-C (which cuts on the carboxyl side of lys) gave rise to a plethora of fragments ranging from at least 18 kDa to >78 kDa under conditions of partial digestion. These fragments can be mapped at best with an accuracy of ±200−500 Da using acrylamide gels (Figure 3). A computer-generated map of T7 RNAP digest with endo lys-C or clostripain gave rise to thousands of possible fragments. For example, the smallest discernible endoproteinase lys-C (or clostripain) fragments in Figure 3 were 22, 20.5, and 18K kDa. (Note that the masses in Figure 3 were given after subtracting the mass of the 23 nt DNA.) In the computer-generated endo lys-C mass bank of peptides, there

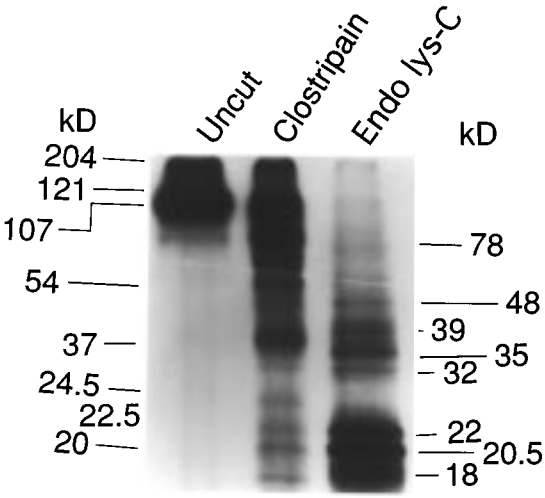

FIGURE 3: Proteolysis of cross-links obtained with −3 IU promoter. The figure shows a typical tris-gly SDS−10% acrylamide gel containing cross-link samples that were digested with two proteases. The numbers indicate the positions of markers (left) and the proteolytic fragments (right).

are 10 fragments in the 22−22.5 kDa size range, 17 fragments in the 20.2−20.8 kDa size range, and 10 fragments in the 18−18.2 kDa size range. All these fragments could potentially fall within the resolution of the gel. The assignment became even more complicated when trypsin, which cuts on the carboxyl side of both Arg and/or Lys, was used. Clearly, high-resolution cross-link mapping using gel electrophoresis alone was of very little use in the case of T7 RNAP. However, when the results from MALDI-TOF, amino acid composition analysis, and gel electrophoresis were used in combination, we were able to map the cross-linked fragments with a high degree of confidence. This procedure was carried out in the following manner.

Cross-linking was carried out on a large scale (10−20 mg of T7 RNAP/batch). The cross-linked material was precipitated with ammonium sulfate to remove most of the non-cross-linked DNA, and the precipitates were run on preparative polyacrylamide−SDS denaturing gels. The bands containing the ^{32}P-labeled cross-linked T7 RNAP were identified by autoradiography of the wet gels. This material was similar to the cross-link band seen in lane 1 (uncut) of Figure 3. The radioactive gel pieces were cut out from the gels and soaked in a buffer solution containing trypsin (see Materials and Methods). After prolonged digestion, the peptides were electroeluted from the gel pieces. The peptides containing the cross-linked DNA were specifically purified in two steps. First, they were adsorbed on to quaternary amine membrane filters and the non-cross-linked peptides were mostly washed away with a low-salt solution. The cross-linked peptides were eluted with a high-salt solution and further purified by anion-exchange HPLC procedures that were similar to those described previously (*31*, *32*). The HPLC was repeated several times to accumulate sufficient −3 IU promoter-T7 RNAP cross-links for the purpose carrying out mass spectrometry and amino acid composition analysis of peptides. Figure 4A shows the anion-exchange HPLC traces of the second step purification of cross-linked peptide(s) that were obtained from trypsin digestion of cross-links between the −3 IU promoter and T7 RNAP. We monitored the absorbance at different wavelength signals and carefully analyzed the absorption spectrum of each HPLC peak

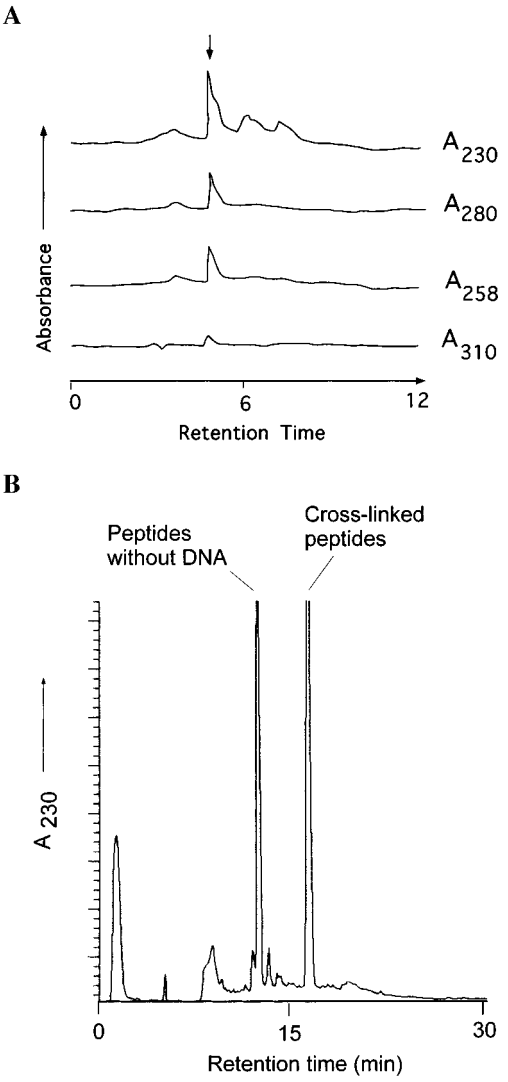

FIGURE 4: (A) Isolation of the −3 IU cross-linked peptides by HPLC. The HPLC method was as follows. Buffer A: 10 mM sodium phosphate (pH 6.7) + 20% acetonitrile. Buffer B: 400 mM sodium phosphate (pH 6.7) + 20% acetonitrile. Buffer B (0−100%) linear ramp in 12 min and 2 mL fractions were collected. The arrow shows the elution position of the cross-links. (B) Separation of naked peptides from cross-linked peptides. Samples of the cross-links were treated with acid as described in the text and purified by C18 reversed-phase. The HPLC method was as follows. Buffer A: 0.1 M TEAA (pH 7.0) in water. Buffer B: 0.1 M TEAA (pH 7.0) + 80% acetonitrile. Buffer B (0−100%) linear ramp in 30 min and 1 mL fractions were collected. The fractions were lyophilized and subjected to microchemical procedures as described in refs *31* and *32*).

and counted the ^{32}P signal from the DNA in the same peak. Using this information, the peak fraction of interest (indicated by the arrow in Figure 4A) was collected. The presence of the DNA in this peak fraction was confirmed by the presence of the ^{32}P label and the broad transition between 260−280 nm in the absorption spectrum that is usually expected for a peptide−DNA conjugate (data not shown).

To facilitate the identification of the peptides by mass spectrometry, we delinked the DNA from the peptides by acidifying (pH 2−3) the cross-links with 0.1% TFA at 37 °C for 4−10 h. Following this procedure, the material was further purified by reversed-phase−ion pair HPLC (Figure 4B). This procedure resulted in about 50% of the peptides without DNA, an estimate that was based on the intensity of HPLC peaks (Figure 4B) and the absorption spectra of the peaks. The DNA delinking reaction could have occurred by either a cleavage of the cross-link and/or by cleavage near an anomeric carbon in the nucleic acid base.[2] In our experience, this procedure was necessary because the peptides and DNA generally carry opposite charges, and the matrices and ionization conditions for obtaining optimal MALDI spectral signals with peptides are different from those used for DNA. The naked peptides were then subjected to MALDI-TOF and to amino acid composition analysis. Figure 5 is a mass spectrum of the peptides from the −3 cross-link. There are four major discernible mass peaks in the mass spectrum, viz., 7070, 5464, 3986, and 2612. These mass determinations are accurate to less than ±5 amu. These fragments matched with the following strings of amino acid residues: 577−642 (obs. mass = 7070; exp. mass = 7070), 577−627 (obs. mass = 5464; exp. mass = 5461), 614−647 (obs. mass = 3986; exp. mass = 3980), and 609−632 (obs. mass 2612; exp. mass 2607). These assignments are based on the assumption that there was a conservation of mass after the photochemistry and the reversal of the DNA from peptides. The following was the determined amino acid composition (avg. mol. %). The actual numbers from the sequence are given in parentheses: A (9.4) 10.0; C (0) 0; Asx (D + N) (13.8) 16.8; Glx (E + Q) (13.4) 15.6; F (0) 0; G (9.2) 13.8; H (0) 0; I (4.7) 5.8; K (6.2) 7.2; L (7.8) 10.2; M (1.6) 1.9; P (0) 0; R (3.1) 2.9; S (6.3) 6.4; T (12.5) 18.3; V (12.5) 16.4; W (1.6) not determined; Y (3.1) 3.1. The determined amino acid composition matched the expected composition to a very good approximation within the acceptable error for quantitative determinations (ca. 10%). Some amino acids are represented in greater quantities than expected, probably because of the presence of minute amounts of contaminating peptides. An important sign is that F, C, and P were absent in the determined composition, as expected, and that the observed number of Y matched with the expected number. Some amino acids (e.g., W) are difficult to quantitate because they are unstable or destroyed. G is generally overrepresented in protein−nucleic acid conjugates. Estimations of (E + Q) and (D + N) are often complicated by deamidation of the amide residues during acid hydrolysis and by poor recoveries (*57*).

We identified the cross-linked fragments based on the following rationale. (1) Since cross-linking probably occurred at a single amino acid residue, all the major peptides in the mass spectrum should overlap in their primary sequence because they represent the same cross-linked site. This inference is reasonable based on the fact that a single discrete band representing the −3 cross-link was always seen in SDS−acrylamide gels indicating a homogeneous product (e.g., see Figure 2B and Figure 3, lane 1). The well-characterized photochemistry of IU results in a single cross-link per IU residue (see the introductory portion of this article and the first paragraph of the Results, and the refs. therein). (2) The intensity of the mass peaks in the spectrum was inversely proportional to the size of the fragments (Figure 5). After extensive digestion of the cross-links over a long period of time (see Material and Methods), one would expect the distribution of fragments to be skewed toward smaller-

[2] Personal communication from Dr. Tad Koch, University of Colorado at Boulder, CO.

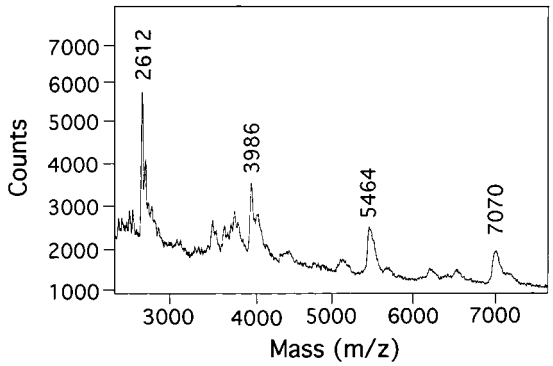

FIGURE 5: MALDI-TOF mass spectrum of the purified peptides that were cross-linked to the −3 IU.

sized fragments over the larger ones (e.g., see Figure 3, lane 3). The intensity of each peak from a separate peptide molecular ion species is somewhat representative of the relative weighted average proportion of that peptide in the mixture. (We hasten to add that MALDI signals cannot be translated into an absolute quantitative measure of the relative amounts of peptides.) (3) The computer-generated masses of a great majority of partial and complete tryptic peptides could not be matched with the observed masses because they were totally outside the range of accuracy of our mass determinations. Therefore, these peptides were ruled out from consideration. There were many other peptides that came closer, within ±30−50 amu of the observed masses. These peptides were also not considered because their end points did not overlap with each other, and when they did overlap, the peptides did not match the masses in the observed mass spectrum within the accuracy of our mass determinations. These categories of peptides were also not considered further. (4) To confirm the identity of the peptides, amino acid composition analysis of a purified cross-link was carried out. The determined amino acid composition of the major peptides agreed with that of the peptide (residues 577−642) containing the cross-link. From the above reasoning, it implies that the 609−632 fragment may indeed be the smallest cross-linked fragment. Furthermore, since the C-terminus of the peptide with a mass of 5464 was residue 627, the N-terminus of peptide with mass of 3986 was

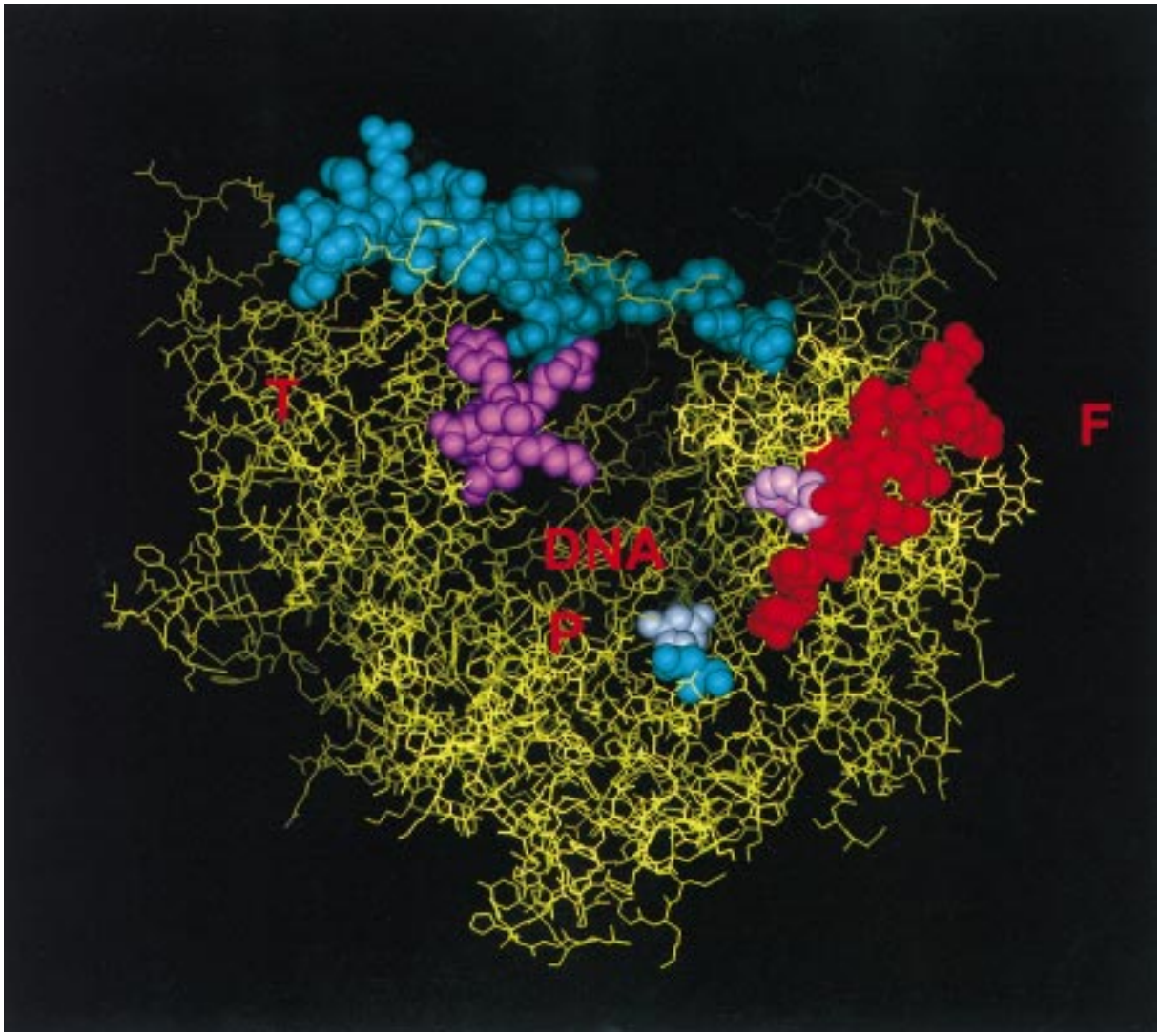

FIGURE 6: The crystallographic model of T7 RNA polymerase was displayed on a Silicon Graphics workstation using INSIGHT II program. The coordinates are from (*26*). The molecule is shown in yellow sticks. F = fingers subdomain; P = palm subdomain; T = thumb subdomain. The position of the promoter is shown in the cleft (DNA). The trajectory of the DNA is perpendicular to the paper. Important regions contacting DNA are shown as van der Waals spheres. The region mapped in this work is in red; Y623 is in light purple; specificity loop is in dark turquoise; active site D537 and D812 are in dark blue and gray, respectively; the contact in the thumb subdomian is in deep purple.

residue 614, and the N-terminus of the peptide with a mass of 2612 was residue 609, the cross-link must be located between residues 609 or 614 and residue 627. The photochemistry of IU cross-linking is very specific to Tyr and, to a much lesser extent to Phe, His, and Met (*51*). No other amino acids have been known to cross-link with IU because of its peculiar photoreactive mechanism. Reading the sequence of T7 RNAP from residue 614 to 627, we noticed that there is only one Tyr at position 623, but there was neither a Phe, a His, nor a Met. This conclusion was also supported by the determined amino acid composition. [The Met(s) are from the rest of the sequences from the peptide mixture.] Therefore, it is most likely that Y623 may have been cross-linked to −3 IU on the template strand. Returning to Figure 3 (endo Lys-C lane), we can now assign the fragments. We observed that the most intense bands were 22, 20.5, and 18 kDa. Among these three bands, the 20.5 kDa fragment was the tightest and the most intense, suggesting that the cross-link must be in this fragment. The 20.5 kDa fragment most probably was from residues 611 to 793, the 22 kDa fragment was probably from residues 442−642 and the 18 kDa fragment was probably from 577 or 578 to 740 or 741. The observed masses deduced from the gel exactly match the calculated masses.

Figure 6 shows the recent crystallographic model of T7 RNAP (*26*). A cocrystal structure of T7 RNA polymerase bound to a promoter has been solved by Dr. Thomas Steitz and his colleagues.[3] The crystallographic model of the polymerase is shaped like a partly open right-hand with a fingers (F, right side), palm (P, center), and thumb (T, left side) subdomains (*26*). The residues 611−627 are shown as red spheres in the fingers subdomain. Unfortunately, residues 609 and 610 could not be placed because they appeared to be disordered in the electron density maps. The light purple spheres sticking out of the patch of red spheres indicates Y623. The fingers subdomain forms a wall of the palm subdomain and rises above the cleft, wherein lies the promoter (marked "DNA" in Figure 6). The active site is indicated by D537 (dark blue spheres) and D812 (gray spheres). A portion of the DNA lies on top of the specificity loop (turquoise spheres at the top of the picture, Figure 6), which penetrates the major groove in the neighborhood of −10 or −8 (*20*, *25*, *49*). Another important contact for stability is probably in the thumb subdomain, residues 369−390 (*29*) (shown as deep purple spheres, Figure 6). As shown in this view (Figure 6), the upstream promoter DNA makes contact with specificity loop and the DNA dips into the active site downstream (downstream +1 site is probably near the conserved D537/D812). We propose that residues 609−627 interact with the melting domain and that, specifically, Y623 may contact or is close to the −3 position of the promoter in a melted configuration. The +1 position is probably close D537 and D812 (which were proposed to ligate with divalent Mg^{2+} ions coordinated to NTP or may ligate to free ions) in the catalytic center. By inference, the −3 contact should be made by Y623, upstream of the +1 start site. Since residues 609−627 (or more specifically Y623) are located above D537 and D812, it is possible that residues 609−627 may be conformationally flexible to contact or to move in the vicinity of the upstream −3 position (Figure 6). Recent crystal structures of ternary complexes of HIV-1 reverse transcriptase and Taq DNA polymerase suggest that the fingers subdomain undergoes a significant conformational change leading to movement of the fingers closer to the palm subdomain, effectively closing off the cleft (*58*, *59*). Such a conformational readjustment may also be visualized for T7 RNAP. This supposition is reasonable because T7 RNAP fingers appear to be taller than those of the Klenow fragment of polI or the HIV reverse transcriptase (*26*, *60*, *61*), which may increase their flexibility. Alternatively, the DNA bubble (including the −3 base) in the open complex may be wide enough or may be somehow bent or distorted in an upward fashion to contact the region shown in red in Figure 6. Mutagenesis of neighborhood residues R627, K631, T636, Y639, G640, and F644 indicated that this region was involved in catalysis (*29*, *62*, *63*). An insertion mutation near codon 610 (K610) somewhat reduced promoter binding (*64*).

[3] Personal communication from Dr. Thomas A. Steitz, Yale University, New Haven, CT.

ACKNOWLEDGMENT

We thank Dr. David Jeruzalmi for supplying the T7 RNAP crystallographic coordinates, Dr. B. T. Chait for suggestions/discussions regarding mass spectrometry, the protein/DNA technology center at the Rockefeller University for help with mass spectrometry and amino acid analysis, and Prof. Joshua Lederberg for his general interest and support.

REFERENCES

1. McAllister, W. T. (1993) *Cell. Mol. Biol. 39*, 385−391.
2. Chamberlin, M. J., and Ryan, T. (1982) *The Enzymes* (Boyer, P. D., Ed.) Vol. 15, pp 87−108, Academic Press, New York.
3. Dunn, J. J., and Studier, F. W. (1983) *J. Mol. Biol. 166*, 477−535; Dunn, J. J., and Studier, F. W. (1984) *J. Mol. Biol. 175*, 111−112 (erratum).
4. Gunderson, S. I., Chapman, K. A., and Burgess, R. R. (1987) *Biochemistry 26*, 1539−1546.
5. Sastry, S. S., and Ross, B. M. (1997) *Biochemistry 36*, 3133−3144.
6. Sastry, S. S., and Ross, B. M. (1996) *Biochemistry 35*, 15715−15725.
7. Diaz, G. A., Rong, M., McAllister, W. T., and Durbin, R. (1996) *Biochemistry 35*, 10837−10843.
8. Ujvari, A., and Martin, C. T. (1996) *Biochemistry 35*, 14574−14582.
9. Jia, Y., Kumar, A., and Patel, S. (1996) *J. Biol. Chem. 271*, 30451−30458.
10. Ikeda, R., Lin, A. C., and Clarke, J. (1992) *J. Biol. Chem. 267*, 2640−2649.
11. Ikeda, R. A., Chang, L. L., and Warshmanna, G. S. (1993) *Biochemistry 32*, 9115−9124.
12. Chapman, K. A., Gunderson, S. I., Anello, M., Wells, R. D., and Burgess, R. R. (1988) *Nucleic Acids Res. 16*, 4511−4524.
13. Muller, D. K., Martin, C. T., and Coleman, J. E. (1989) *Biochemistry 28*, 3306−3313.
14. Rastinejad, F., and Lu, P. (1993) *J. Mol. Biol. 232*, 105−122.
15. Stahl, S. J., and Chamberlin, M. J. (1978) *J. Biol. Chem. 253*, 4951−4959.
16. Chapman, K. A., and Burgess, R. R. (1987) *Nucleic Acids Res. 15*, 5413−5432.
17. Ikeda, R. A., Warshanna, G. S., and Chang, L. (1992) *Biochemistry 31*, 9073−9080.
18. Diaz, G. A., Raskin, C. A., and McAllister, W. T. (1993) *J. Mol. Biol. 229*, 805−811.
19. Li, T., Ho, H. H., Maslak, M., Schick, C., and Martin, C. T. (1996) *Biochemistry 35*, 3722−3727.
20. Rong, M., He, B., McAllister, W. T., and Durbin, R. K. (1998) *Proc. Natl. Acad. Sci. 95*, 515−519.

21. Schick, C., and Martin, C. T. (1995) *Biochemistry 34*, 666−672.
22. Weston, B. F., Kuzmine, I., and Martin, C. T. (1997) *J. Mol. Biol. 272*, 21−30.
23. Osterman, H. L., and Coleman, J. E. (1981) *Biochemistry 20*, 4884−4892.
24. Villemain, J., Guajardo, R., and Sousa, R. (1997) *J. Mol. Biol. 273*, 958−977.
25. Sousa, R., Chung, Y. J., Rose, J. P., and Wang, B.-C. (1993) *Nature (London) 364*, 593−599.
26. Jeruzalmi, D., and Steitz, T. A. (1998) *EMBO J. 17*, 4101−4113.
27. Joyce, C. M., and Steitz, T. A. (1994) *Annu. Rev. Biochem. 63*, 777−822.
28. Joyce, C. M., and Steitz, T. A. (1995) *J. Bacteriol. 177*, 6321−6329.
29. Bonner, G., Lafer, E. M., and Sousa, R. (1994) *J. Biol. Chem. 269*, 25129−25136.
30. Sousa, R., Rose, J., and Wang, B. C. (1994) *J. Mol. Biol. 244*, 6−12.
31. Sastry, S. S. (1996) *Biochemistry 35*, 13519−13530.
32. Sastry, S. S., Spielmann H. P., Hoang Q. S., Phillips, A. M., Sancar, A., and Hearst, J. E. (1993) *Biochemistry 32*, 5526−5538.
33. Sastry, S., and Ross, B. M. (1998) *Proc. Natl. Acad. Sci. U.S.A. 95*, 9111−9116.
34. Sastry, S. S., Spielmann, H. P., Dwyer, T. J., Wemmer, D. E., and Hearst, J. E. (1992) *J. Photochem. Photobiol. B. 14*, 65−79.
35. Maniatis, T., Fritsch, E. F., and Sambrook, J. (1982) *Molecular cloning: a laboratory manual*, Cold Spring Harbor Laboratory, Plainview, NY.
36. Grodberg, J., and Dunn, J. J. (1988) *J. Bacteriol. 170*, 1245−1253.
37. Zawadzki, V., and Gross, H. J. (1991) *Nucleic Acids Res. 19*, 1948.
38. Maslak, M., and Martin, C. T. (1994) *Biochemistry 33*, 6918−6924.
39. Beavis, R. C., and Chait, B. T. (1996) *Methods Enzymol. 270*, 519−551.
40. Beavis, R. C., and Chait, B. T. (1990) *Anal. Chem. 62*, 1836−1840.
41. Pendergrast, P. S., Chen, Y., Ebright, Y. W., and Ebright, R. H. (1992) *Proc. Natl. Acad. Sci. U.S.A. 89*, 10287−10291.
42. Chen, A., Powell, L. M., Dryden, D. T. F., Murray, N. E., and Brown, T. (1995) *Nucleic Acids Res. 23*, 1177−1183.
43. Pandey, V. N., Kaushik, N., and Modak, M. J. (1994) *J. Biol. Chem. 269*, 21828−21834.
44. Willis, M. C., Hicke, B. J., Uhlenbeck, O. C., Cech, T. R., and Koch, T. H. (1993) *Science 262*, 1255−1257.
45. Willis, M. C., LeCuyer, K. A., Meisenheimer, K. M., Uhlenbeck, O. C., and Koch, T. H. (1994) *Nucleic Acids Res. 22*, 4947−4952.
46. Norris, C. L., Meisenheimer, P. L., and Koch, T. H. (1996) *J. Am. Chem. Soc. 118*, 5796−5803.
47. Muller, D. K., Martin, C. T., and Coleman, J. E. (1988) *Biochemistry 27*, 5763−5771.
48. Maslak, M., Jaworski, M. D., and Martin, C. (1993) *Biochemistry 32*, 4270−4274.
49. Raskin, C. A., Diaz, G. A., Joho, K. E., and McAllister, W. T. (1992) *J. Mol. Biol. 228*, 506−515.
50. Ikeda, R., Ligman, C. M., and Warshamana, S. (1992) *Nucleic Acids Res. 20*, 2517−2524.
51. Meisenheimer, K. M., and Koch, T. H. (1997) *Crit. Rev. Biochem. Mol. Biol. 32*, 101−104.
52. Dietz, T. M., and Koch, T. H. (1987) *Photochem. Photobiol. 46*, 971−978.
53. von Hippel, P. H., and Schleich, T. (1969) in *The structure and stability of biological macromolecules* (Timaschef, S. T., and Fasman, G. D., Eds.) pp 417−574, Marcel Dekker. Inc., New York.
54. Collins, K. M., and Washabaugh, M. W. (1985) *Q. Rev. Biophys. 18*, 323−422.
55. Lohman, T. M. (1986) *CRC Crit. Rev. Biochem. 19*, 191−245.
56. Record, M. T. J., Anderson, C. F., and Lohman, T. M. (1978) *Q. Rev. Biophys. 11*, 103−178.
57. Blackman, S. e. (1978) *Amino acid determination: methods and techniques*, pp 8−35, Marcel Dekker, New York.
58. Li, Y., Korolev, S., and Waksman, G. (1998) *EMBO J. 17*, 7514−7525.
59. Huang, H., Chopra, R., Verdine, G. L., and Harrison, S. C. (1998) *Science 282*, 1669−1675.
60. Ollis, D. L., Brick, P., Hamlin, R., Xuong, N. G., and Steitz, T. A. (1985) *Nature 313*, 762−766.
61. Kohlstaedt, L. A., Wang, J., Friedman, J., Rice, P. A., and Steitz, T. A. (1992) *Science 258*, 1783−1790.
62. Bonner, G., Patra, D., Lafer, E. M., and Sousa, R. (1992) *EMBO J. 11*, 3767−3775.
63. Osumi-Davis, P., Sreerama, N., Volkin, D. B., Middaugh, C. R., Woody, R. W., and Woody, A.-Y., M. (1994) *J. Mol. Biol. 237*, 5−19.
64. Gross, L., Chen, W. J., and McAllister, W. T. (1992) *J. Mol. Biol. 228*, 488−505.

BI9823941